Desalination and Water Treatment
www.deswater.com
doi: 10.5004/dwt.2020.26460

208 (2020) 423–433
December

Comparative study of solar-Fenton: catalytic degradation of pure and impure biotemplated $BiFeO_3$ nanocatalyst towards 4-chlorophenol

Noor Haida Mohd Kaus[a,*], Yi Thing Khor[a], Rohana Adnan[a], Hooi-Ling Lee[a], Mohd Lokman Ibrahim[b,c], Nor Atilia Athira Zaahari[a], Mohamad Haafiz Mohamad Kassim[d]

[a]*School of Chemical Sciences, Universiti Sains Malaysia, 11800 Penang, Malaysia, emails: noorhaida@usm.my (N.H. Mohd Kaus), yithingkhor.arus@gmail.com (Y.T. Khor), r_adnan@usm.my (R. Adnan), hllee@usm.my (H.L. Lee), atiliazahari@usm.my (N.A. Athira Zaahari)*
[b]*Centre for Nanomaterials Research, Institute of Science, Level 3, Block C, UiTM Shah Alam, Selangor, Malaysia, email: lokman547@gmail.com (M.L. Ibrahim)*
[c]*School of Chemistry and Environment, Faculty of Applied Science, UiTM Shah Alam, Selangor, Malaysia*
[d]*School of Industrial Technology, Universiti Sains Malaysia, 11800 Penang, Malaysia, email: mhaafiz@usm.my (M.H. Mohamad Kassim)*

Received 1 February 2020; Accepted 14 August 2020

ABSTRACT

This study has successfully demonstrated the formation of pure and impure bismuth ferrite ($BiFeO_3$) photocatalyst produced using alginic acid as a biotemplate. Structural and phase purity of the nanocatalysts were tested, and efficiencies of both pure and impure $BiFeO_3$ nanocatalysts in 4-chlorophenol (4-CP) degradation were conducted via solar-Fenton reaction. Catalytic activities were investigated with respect to the initial concentrations of 4-CP and oxidant, H_2O_2, nanocatalyst loading and reaction time. The Langmuir-Hinshelwood kinetic model is best suited to the degradation activity. High purity $BiFeO_3$ nanocatalyst exhibited high photodegradation activity with low dosage as well as high stability, surface area and ability to regenerate compared to impurity $Bi_2Fe_4O_9$. Results showed ~98% degradation of 200 mg L^{-1} of 4-CP at pH 2.5 with 0.1 mol L^{-1} of H_2O_2 and 2.55 mmol L^{-1} of nanocatalyst within 180 min and no significant reduction in terms of its reusability. The influence on phase purity and the structural properties of the photocatalyst is significant for providing opportunities in developing an intensive study in an environmentally friendly solar photocatalyst.

Keywords: Bismuth ferrite nanocatalyst; 4-chlorophenol; Biotemplate; Alginic acid; Solar-Fenton reaction

1. Introduction

Chlorophenols (CPs) are commonly known to be extremely toxic and not easily degradable. Some chlorinated compounds are biodegradable, however, their kinetics are often slow and biodegradation of the compounds is possible only at low concentration [1,2]. These chlorinated compounds with the safety level of 0.1–1.0 mg L^{-1} [3,4] are categorized as a particular group of priority toxic compounds by the United States Environmental Protection Agency (USEPA) [5]. These essential pollutants can be found through many manufacturing activities such as petroleum refineries, bleaching of paper pulp, water disinfection, and excessive use of pesticides and herbicides [6,7]. Apart from being considered as environmental pollutions, CPs often affect human health with diseases such as liver malfunction and dermatitis [1]. Hence, in recent decades, the sustainability approach in the removal of chlorinated phenolic compounds from industrial wastewater has generated considerable attention from the community [8].

* Corresponding author.

1944-3994/1944-3986 © 2020 Desalination Publications. All rights reserved.

Heterogeneous semiconductor photocatalysis which acts as versatile, low cost, and environmentally benign treatment technology for a host of pollutants have emerged as a promising solution in the mineralization of organic pollutants in water. The process involves surface trapping of light-generated charges which induce interfacial electron-transfer reactions with a great variety of substrates [9,10]. Titanium dioxide (TiO_2) based photocatalysts have been extensively studied by conducting various investigations focusing on two main forms of TiO_2, namely rutile (bandgap 3.0 eV), anatase (bandgap 3.2 eV) and brookite (bandgap 3.13 eV) [11–16]. The large bandgap of TiO_2 barely responses to UV light (<380 nm), which accounts for less than 4% of the entire solar spectrum [17] and hence, it limits the effective use of solar energy. This has consequent implications for the use of titania materials as solar or room light-activated catalysts. Several studies conducted on visible-light-induced photocatalysis such as $ZnFe_2O_4$ [18], $PW_{11}Fe/H_2O_2$ [19], and C/ZnO/CdS [20] have demonstrated their photocatalytic efficiency and further supported a more sustainable approach towards the chemical utilization of solar light.

Therefore, it is of great interest to develop an efficient solar-light photocatalyst for the photodegradation of organic pollutants with two key factors affecting the photocatalytic performance that are the solar-light response and the separation of photogenerated electron-hole pair. Therefore, bismuth ferrite, $BiFeO_3$ which possesses a rhombohedral distorted perovskite structure with a narrow bandgap (2.1 eV) and high chemical stability [21] has been selected as the alternative photocatalyst in this study. Based on the fact that $BiFeO_3$ possesses a narrower bandgap compared to many other ferroelectric perovskites, therefore, it is responsive towards a wide spectrum of solar light including visible light and UV light. Furthermore, multiferroic $BiFeO_3$ is also known to have a high separation efficiency of photogenerated electron and hole due to the self-polarization field, which is caused by self-polarization in ferromagnetic mechanism [22], thus becoming a great interest in photocatalysis [23,24].

Nevertheless, the synthesis of $BiFeO_3$ with high temperature and low purity is often complex due to its narrow temperature range of phase stabilization [25]. Extensive researches have been conducted by undergoing a lower temperature synthesis path to overcome the problems of poor reproducibility and poor ferroelectric behavior [26]. The biotemplating technique with biopolymers and polysaccharides is a greener approach is considered as an environmentally and economically friendly because the process takes place under a milder condition and allows greater morphological control in producing high purity crystal. alginic acid polysaccharides are naturally found on the cell walls of brown algae, which are made up of blocks of polyguluronate, poly-G and poly-M blocks. The poly-G blocks are able to strongly bind cations that serve as the preferential sites for nucleation and growth of metal cations, while also avoiding coalescence of nanoparticulate species [27]. In the synthesis of $BiFeO_3$, poly-G blocks act as a structure-directing agent in the assembly of $BiFeO_3$ nanostructure [28].

Several studies have reported the effectiveness of impure $BiFeO_3$ compared to high purity $BiFeO_3$ despite the complicated process involved in the synthesis of high purity $BiFeO_3$ such as $BiFeO_3$ with impurity phases ($Bi_2Fe_4O_9$, $Bi_{25}FeO_{40}$, and Bi_2O_3-Fe_2O_3) [29]. The type of impurities phases plays a significant role in order to further catalyze the photocatalytic processes. Hence, the effectiveness of $BiFeO_3$ with impurities phases (Bi_2O_3 and Fe_2O_3) was the result of the presence of ferrous oxide impurities which further catalyze the Fenton reaction by converting Fe^{3+} to Fe^{2+}, in order to generate hydroxyl radicals ($^{\bullet}OH$) for solar-Fenton catalytic degradation of phenolic compounds.

In this study, the effectiveness of the composition of impurity $Bi_2Fe_4O_9$ in $BiFeO_3$ synthesized through the green approach utilizing the polysaccharide alginic acid is examined and compared to the high purity $BiFeO_3$ nanocatalyst under solar-Fenton catalytic degradation of 4-chlorophenol (4-CP). Besides, several other aspects were evaluated including the effects of pH, the initial concentration of 4-CP, the concentration of the oxidant (H_2O_2), the dosage of $BiFeO_3$, the reaction time, and the regeneration study.

2. Experimental setup

2.1. Chemical and materials

All chemicals applied in the experiments were of reagent grade or higher and used without further purification. Bismuth nitrate [$Bi(NO_3)_3{\cdot}5H_2O$], iron nitrate [$Fe(NO_3)_3{\cdot}9H_2O$] from Sigma-Aldrich (USA), and alginic acid from Acros Organics (USA) have been used in the synthesis of pure and impure $BiFeO_3$ nanocatalysts. 4-CP was obtained from Aldrich. Hydrogen peroxide (H_2O_2) and hydrochloric acid (HCl) were obtained from QReC, while ammonium hydroxide was supplied by J.T. Baker (USA).

2.2. Characterisation of pure and impure $BiFeO_3$ nanocatalyst

Pure and impure $BiFeO_3$ samples were analyzed using X-ray diffraction (XRD). The XRD patterns were recorded with a PANalytical X'Pert PRO θ-2θ, which is equipped with graphite monochromatized using CuKα radiation (λ = 1.54060 Å) operating at 40 kV. With reference to the Debye Scherrer's equation, the crystallite size is calculated using the Eq. (1):

$$D = \frac{k\lambda}{B\cos\theta} \tag{1}$$

where B is the full width at half maximum of intensity (in radian) vs. 2θ profile, λ is the wavelength of the CuKα radiation (1.5406 Å), θ is the Bragg's diffraction angle, D is the crystallite size, and k is a constant that depends on the shape of the crystallite size and equals to 0.9. The Scherrer equation is not applicable to grains that are larger than 0.1 μm; hence, it is limited to the measurement of nanoscale particles only.

The morphology of the sample was studied using the scanning electron microscopy with a scanning microscope

FEI QUANTA FEG 650 coupled with energy-dispersive X-ray system Oxford instruments X-MAX (EDX, USA). Chromium was used to coat the sample before the characterization. Brunauer–Emmett–Teller (BET) surface areas were obtained using porosimeter Micromeritics ASAP 2020.

2.3. Preparation of pure and impure $BiFeO_3$ nanocatalyst

In the common procedure conducted to prepare pure $BiFeO_3$ nanocatalyst, 1.42 g of $[Bi(NO_3)_3{\cdot}5H_2O]$ and 2.00 g of $[Fe(NO_3)_3{\cdot}9H_2O]$ were dissolved in 25 mL distilled water. The solution was then added into the alginic acid polymer and stirred at 80°C for 2 h. Ammonium hydroxide (NH_4OH) was used to adjust the pH of the mixture to achieve pH 8 until a brownish-red solution was obtained. Consequently, the mixture was dried in an oven overnight. Finally, the gel-like sample was calcined at 550°C for 2 h. Similarly, a 1:1 mole ratio of starting materials 2.42 g of $[Bi(NO_3)_3{\cdot}5H_2O]$ and 2.00 g of $[Fe(NO_3)_3{\cdot}9H_2O]$ were used in the synthesis of impure $BiFeO_3$ nanocatalyst.

2.4. Catalytic activity test

The catalytic activity of pure and impure $BiFeO_3$ nanocatalysts has been evaluated in a heterogeneous photo Fenton catalytic degradation of 4-CP from aqueous solution. In this case, several Erlenmeyer flasks containing 50 mL 4-CP (200 mg L^{-1}), 0.1 M H_2O_2, and 0.04 g of catalyst at pH 2.5 were agitated in the dark for 30 min on a shaker with the mixing rate of 350 rpm. The solutions were then exposed to direct sunlight radiation in consecutive sunny days, which was between 12 P.M. to 4 P.M. (GPS coordinates: N 15′ 47.9442″, E 29′ 4.6356″). The removal efficiency of 4-CP was determined based on the remaining 4-CP concentration at 280 nm using the Shimadzu UV-Vis Model UV-2600 spectrophotometer. For the kinetic study, the solutions are collected every 30 min and analyzed using a UV-Vis spectrophotometer. The percentage of degradation is calculated using the following equation:

$$\%\ \text{Degradation} = \frac{C_0 - C}{C_0} \times 100\% \quad (2)$$

where C_0 is the initial concentration of 4-CP and C is the final 4-CP concentration.

A few parameters including the pH of the medium, the initial concentration of 4-CP, the concentration of H_2O_2 and the dosage of $BiFeO_3$ were evaluated to examine the effectiveness of pure and impure $BiFeO_3$ nanocatalysts. The pH values were adjusted by adding 1.0 M HCl or NaOH.

2.5. Reusability of photocatalyst

The nanocatalysts were collected from the solution using a permanent magnet. The samples were dried in an oven and washed by stirring with 50 mL of distilled water for 180 and 210 min for pure $BiFeO_3$ and impure $BiFeO_3$ nanocatalysts, respectively. The catalysts were then dried again and suspended into a fresh solution of 4-CP and H_2O_2. The degradation activity is continued with the second cycle and the process was repeated.

3. Results and discussion

3.1. Characterization of the catalyst

3.1.1. Phase analysis of biotemplated-$BiFeO_3$ nanocatalyst

As illustrated in Fig. 1a, the XRD pattern of pure $BiFeO_3$ nanocatalyst contains diffracted peaks at 2θ values of 22.41°, 31.99°, 39.46°, 45.81°, 54.03°, 57.08°, 67.10°, 71.80°, and 76.21° which correspond to the (012), (110), (202), (024), (116), (300), (220), (312), and (134) crystal planes of rhombohedral $BiFeO_3$ (JCPDS card No. 01-071-2494). No other peak is observed, thus indicating that the synthesized $BiFeO_3$ nanocatalyst is of high purity, single-phase and the broad peaks represent the smaller crystallite size of the pure $BiFeO_3$ sample. The XRD pattern of impure $BiFeO_3$ nanocatalyst shown in Fig. 1b resonates with the XRD pattern of the pure $BiFeO_3$ nanocatalyst. The dominant peaks of impure $BiFeO_3$ nanocatalyst represent the diffraction of pure $BiFeO_3$ nanoparticles. However, the peaks at 23.90°, 28.15°, 28.99°, 29.46°, 30.28°, 47.03°, and 56.50° belonging to the (120), (121), (211), (002), (220), (141), and (332) crystal planes of orthorhombic $Bi_2Fe_4O_9$ (JCPDS card No. 00-025-0090) were detected in the diffractogram. This indicates that the impure $BiFeO_3$ nanocatalyst comprises rhombohedral $BiFeO_3$ and orthorhombic $Bi_2Fe_4O_9$ nanoparticles. The average crystalline size (Table 1) of pure and impure biotemplated $BiFeO_3$ nanocatalyst calculated using the Debye-Scherrer equation is 16.7 and 52.5 nm, respectively.

3.1.2. Morphology and elemental composition of biotemplated-$BiFeO_3$ nanocatalyst

Figs. 2a and c reveal the morphology of the pure $BiFeO_3$ nanocatalyst consist of a single phase of rhombohedral shape with the particle size of 87.0 ± 30 nm, while the impure $BiFeO_3$ nanocatalyst has the irregular distribution of rod-shaped orthorhombic phase (Figs. 2b and d) with a larger particle size of 184.2 ± 88 nm. This correlates with the XRD patterns (Fig. 1) observed in impure and pure $BiFeO_3$ nanocatalyst, which further confirms the presence of orthorhombic ($Bi_2Fe_4O_9$) and rhombohedral ($BiFeO_3$) particles,

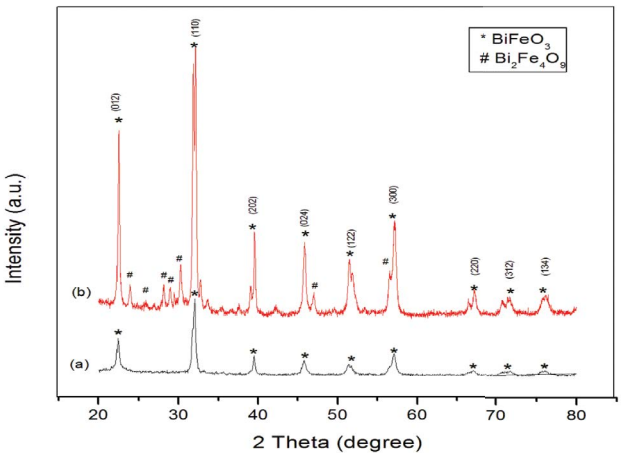

Fig. 1. XRD patterns of (a) pure and (b) impure biotemplated-$BiFeO_3$ nanoparticles.

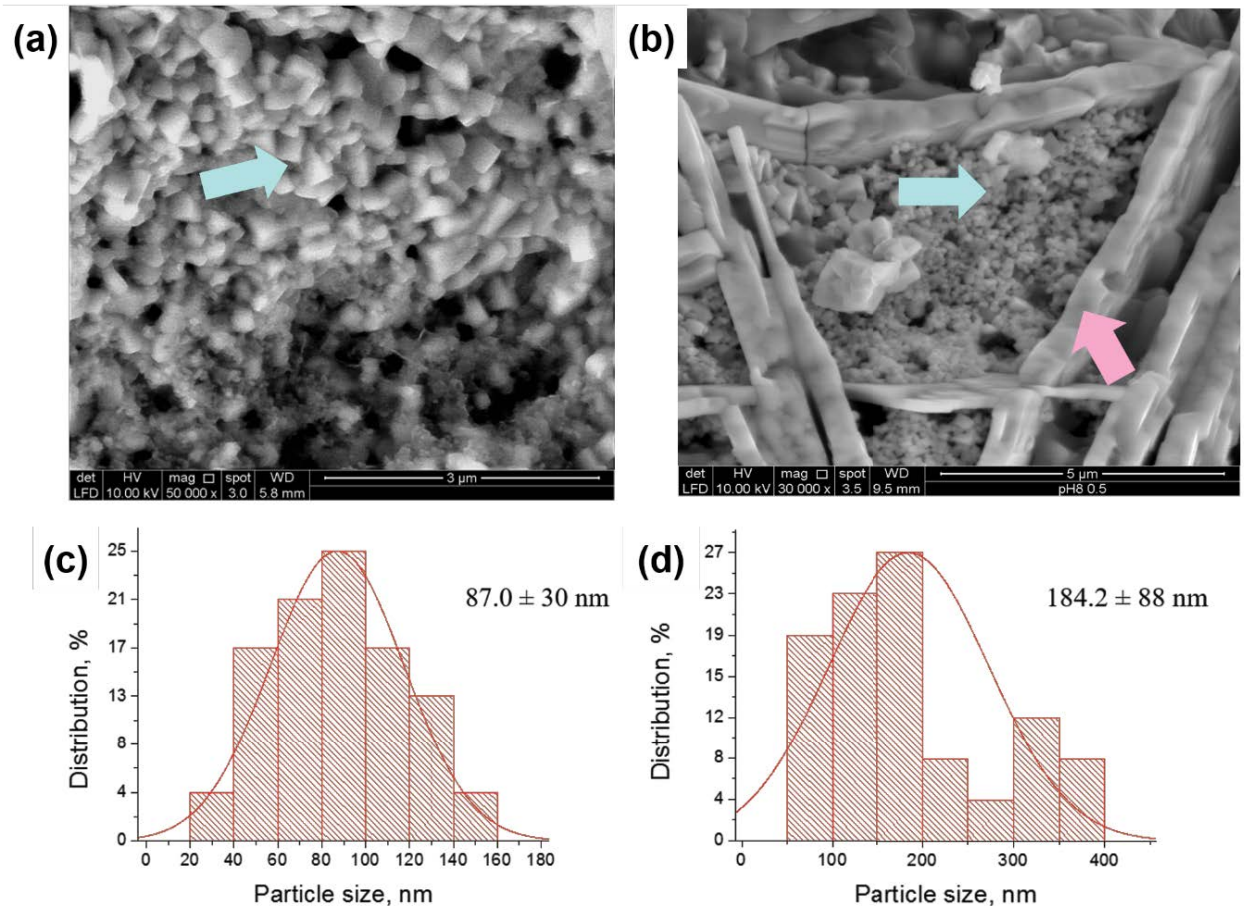

Fig. 2. Field emission scanning electron microscopy images and histogram of the particle size distribution of (a,c) pure and (b,d) impure biotemplated $BiFeO_3$ nanoparticles. Green arrow: rhombohedral phase; pink arrow: rod-shaped orthorhombic phase.

respectively. Summarization of morphologies and crystallite dimensions are tabulated in Table 1. Further characterization of elemental composition was performed using energy-dispersive X-ray analysis for both nanocatalysts (Fig. S1). The transmission electron microscopy image as depicted in (Fig. S2) revealed major agglomeration of the impure ($Bi_2Fe_4O_9$) samples as compared to pure $BiFeO_3$. In addition, pure $BiFeO_3$ experienced better distribution of smaller particles and this will provide more active sites for the reaction and having a high rate of photocatalytic reaction.

3.1.3. BET study of biotemplated-$BiFeO_3$ nanocatalyst

The N_2 adsorption-desorption on both biotemplated $BiFeO_3$ nanocatalyst was carried out. BET analysis was performed, and the result exhibited pure $BiFeO_3$ has a 6-fold higher surface area than the impure ($Bi_2Fe_4O_9$) sample with the values of 12.9891 and 2.9840 $m^2\ g^{-1}$, respectively as tabulated in Table 1. The larger surface area of pure $BiFeO_3$ nanocatalyst is caused by its homogeneity of crystal growth, which provides better orientation of resulting crystallite and higher preferential sites for photocatalytic purposes compared to the impure $BiFeO_3$ nanocatalyst [30]. Therefore, the significantly higher surface area of the pure $BiFeO_3$ nanoparticles with a smaller size is responsible for the presence of more active sites that provided higher degradation efficiency.

3.2. Photocatalytic activity

3.2.1. Effect of 4-CP degradation in dark and under sunlight with and without H_2O_2

The photocatalytic capability of both pure and impure $BiFeO_3$ nanocatalysts was investigated a solar-Fenton catalytic degradation of 4-CP in the presence and absence of H_2O_2. The 4-CP degradation by pure and impure $BiFeO_3$ nanocatalysts in the presence of 0.1 mol L^{-1} H_2O_2 were performed under both dark and light condition. It was first evaluated by the degradation of the 4-CP organic contaminant and the observed time-dependent photodegradation of 4-CP under these conditions is illustrated in Fig. 3 and summarised in Table 2. First, it may be noted that under dark and in the absence of H_2O_2, the $BiFeO_3$ nanocatalyst does not cause any discernible degradation of 4-CP over the measurement time-domain (Table 2). Further investigations on the effectiveness of H_2O_2 for both nanocatalysts in the absence of solar light were carried out and illustrated in Fig. 3. The results show there is a low percentage of ~0.48% degradation of 4-CP in the absence of light

Table 1
The physical characteristic of studied $BiFeO_3$ and its photocatalytic activity

Morphology $BiFeO_3$	Crystallite size (nm)	Particles size (nm)	BET surface area ($m^2\ g^{-1}$)	Best dosage of $BiFeO_3$ ($mmol\ L^{-1}$)	Percentage degradation of 200 mg L^{-1} 4-CP (t = 180 min)	Rate of degradation, (min^{-1})
Impure (orthorhombic)	52.5	184.2 ± 88	2.984	6.4	97.0	0.0254
Pure (rhombohedral)	16.7	87.0 ± 30	12.989	2.5	98.0	0.0314

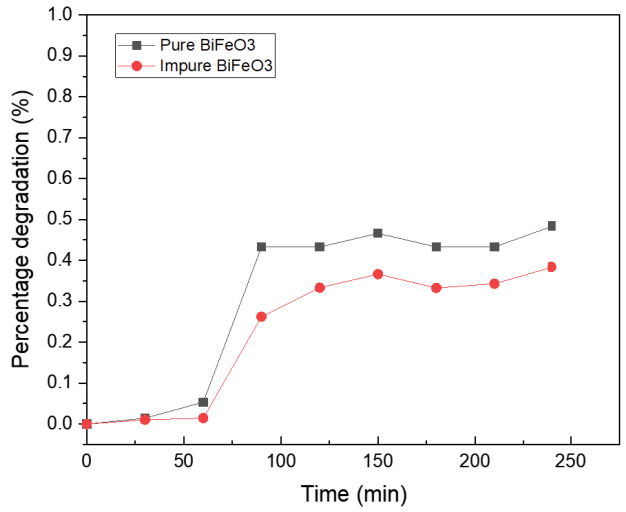

Fig. 3. Effect of degradation of 4-CP under dark condition with pure and impure $BiFeO_3$ nanocatalyst in the presence of H_2O_2. (Pure $BiFeO_3$ = 2.5 mmol L^{-1}; impure $BiFeO_3$ = 6.4 mmol L^{-1}; H_2O_2 = 0.1 mol L^{-1}; pH = 2.5; time = 240 min).

even with the addition of 0.1 M oxidant, H_2O_2. The addition of H_2O_2 leads to a certain rate of degradation even in the dark (Fig. 3) which is the same as that by the use of only H_2O_2 without $BiFeO_3$. This means that H_2O_2 itself causes a slow 4-CP degradation and this can be attributed to the oxidizing nature of H_2O_2. However, as clearly seen from the data shown in the same Table 2, $BiFeO_3$ is clearly and significantly assisted by a similar concentration of H_2O_2, reflecting photo-Fenton catalytic enhancement. The photo-Fenton process, the combination of homogeneous systems of solar/H_2O_2/Fe^{2+} compounds, produces the highest photochemical elimination rate of 4-CP and complete mineralization is possible to achieve in shorter reaction periods when compared with the H_2O_2/Fe^{2+} process in the dark. The result displayed promising photodegradation of 4-CP in the presence of solar light and oxidant.

3.2.2. *Effect of the concentration of H_2O_2 on the solar-Fenton catalytic degradation of 4-CP*

H_2O_2 has been widely reported as an effective oxidant in catalyzing the photocatalytic reaction. Therefore, the optimum concentration of H_2O_2 is evaluated to ensure the minimum use of oxidant in order to achieve high degradation efficiency. The experiments were conducted with different concentrations of H_2O_2, which ranges from 0.06 to 0.10 mol L^{-1}. In Fig. 4, a gradual increase in the percentage of degradation can be observed from lower H_2O_2 concentration at 0.06 mol L^{-1} (7.48% and 6.32%) to higher concentration at 0.10 mol L^{-1} (94.12% and 90.68%) for both nanocatalysts. The results show that higher degradation efficiency is achieved by increasing the concentration of H_2O_2. The increase in activity with light at higher H_2O_2 concentration can be attributed to the combination of nanophotocatalysis and solar-Fenton catalysis processes. Hence, the optimized value of H_2O_2 concentration (0.1 mol L^{-1}) was used for the rest of the study.

Table 2
Effect of $BiFeO_3$ on the catalytic degradation of 4-CP under dark and direct sunlight ($BiFeO_3$ = 2.5 mmol L^{-1}; 4-CP = 200 mg L^{-1}; time = 240 min)

Catalyst	Condition	Time, t (min)	Degradation, %
0.1 M H_2O_2	In the dark	240	N/A
	Under direct sunlight	240	N/A
$BiFeO_3$	In the dark	240	0.75
without H_2O_2	Under direct sunlight	240	1.07
$BiFeO_3$ with	In the dark	240	0.48
0.1 M H_2O_2	Under direct sunlight	240	98.0

3.2.3. *Effect of pH medium on the solar-Fenton catalytic degradation of 4-CP*

The pH of a solution is considered an important parameter because it directly affects the photocatalytic performance of a Fenton reaction due to the fact that this reaction is more effective when conducted under acidic conditions. Fig. 5 depicts the percentage of degradation of 200 mg L^{-1} of 50 mL 4-CP over a wide range of pH. In the same figure, the solar-Fenton catalytic degradation of 4-CP over both pure and impure $BiFeO_3$ nanocatalysts surface is shown to be lower in less acidic and alkaline medium with pH 5.5 and pH 8, respectively. The increase in the percentage of degradation is observed when the solution becomes acidic starting at pH 2 for both pure and impure catalyst, while a dramatic increase in the degradation efficiency (~90%) recorded as was observed at pH 2.5.

Under acidic conditions, $BiFeO_3$ nanocatalysts catalyzed the decomposition of H_2O_2 into $^{\bullet}OH$ radicals. The predominant iron sites, $\equiv Fe^{3+}$ absorbs light to produce $\equiv Fe^{2+}$ and $^{\bullet}OH$ by the initial formation of a complex between $\equiv Fe^{3+}$ and H_2O_2. This critically enhances the degradation process because

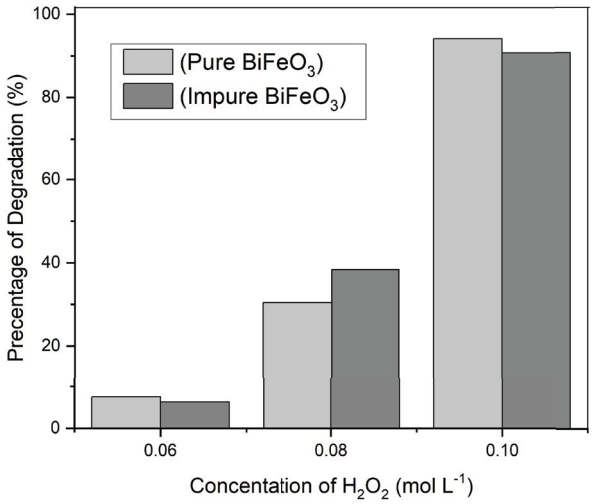

Fig. 4. Effect of concentration of H_2O_2 on solar-Fenton catalytic degradation of 4-CP. (Pure $BiFeO_3$ = 2.5 mmol L^{-1}; impure $BiFeO_3$ = 6.4 mmol L^{-1}; [H_2O_2] = 0.1 mol L^{-1}; [4-CP] = 200 mg L^{-1}; time, t = 180 min).

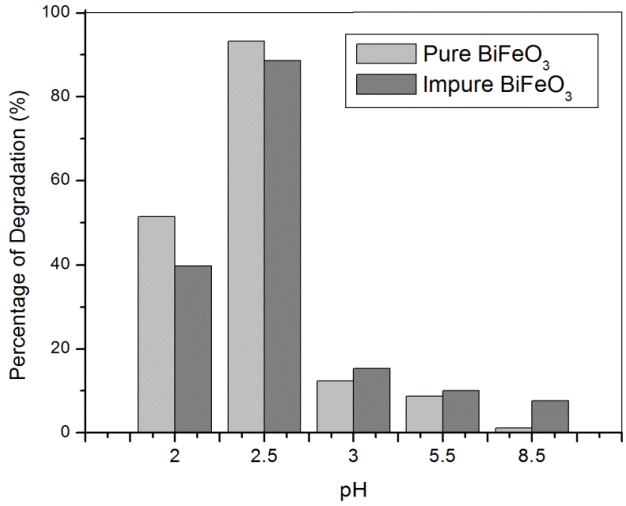

Fig. 5. Effect of pH on solar-Fenton catalytic degradation of 4-CP. (Pure $BiFeO_3$ = 2.5 mmol L^{-1}; impure $BiFeO_3$ = 6.4 mmol L^{-1}; [H_2O_2] = 0.1 mol L^{-1}; [4-CP] = 200 mg L^{-1}; time, t = 180 min).

≡Fe^{2+} acts as the major catalytic species in Fenton reaction while •OH is considered as the active species responsible to attack and degrade the organic materials (Eqs. (3)–(7)).

$$\equiv Fe^{3+} + H_2O_2 \rightarrow \equiv Fe^{3+}H_2O_2 \quad (3)$$

$$\equiv Fe^{3+}H_2O_2 \rightarrow \equiv Fe^{2+} + {}^{\bullet}HO_2 + H^+ \quad (4)$$

$$\equiv Fe^{3+} + {}^{\bullet}HO_2 \rightarrow \equiv Fe^{2+} + O_2 + H^+ \quad (5)$$

$$\equiv Fe^{2+} + H_2O_2 \rightarrow \equiv Fe^{3} + {}^{\bullet}OH + OH^- \quad (6)$$

$$4-CP + {}^{\bullet}OH \rightarrow \cdots CO_2 + H_2O \quad (7)$$

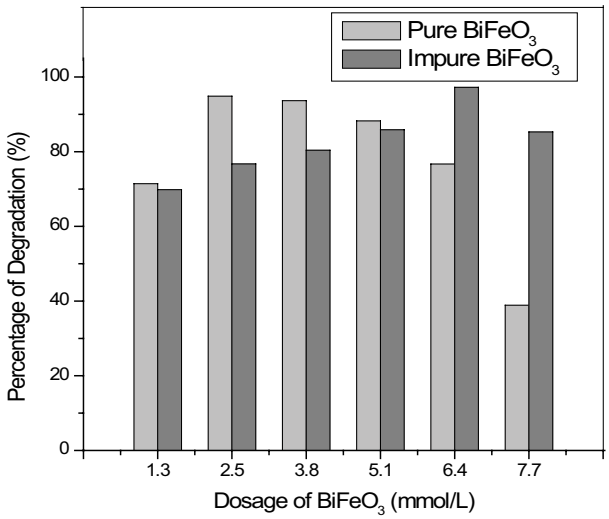

Fig. 6. Effect of dosage of $BiFeO_3$ on solar-Fenton catalytic degradation of 4-CP (H_2O_2 = 0.1 mol L^{-1}; 4-CP = 200 mg L^{-1}; pH = 2.5; time = 180 min).

In alkaline pH, a high valence iron species (Fe^{4+} = O) may form due to the removal of H atom by OH^- species in alkaline conditions (Eq. (8)). It is worth to note that Fe^{4+} = O species are less reactive than •OH and are unable to react with aromatic compounds.

$$\equiv Fe^{2+} + H_2O_2 \rightarrow \equiv Fe^{4+} = O + H_2O \quad (8)$$

where ≡ represents the active sites on the surface of $BiFeO_3$ nanoparticles.

Therefore, based on the findings, the rest of the photocatalytic study was conducted at an optimum pH of 2.5.

3.2.4. Effect of dosage of pure and impure $BiFeO_3$ nanocatalysts on the solar-Fenton catalytic degradation of 4-CP

The optimum dosages of pure and impure $BiFeO_3$ nanocatalysts were evaluated in the range of 1.28–7.7 mmol L^{-1}. Fig. 6 depicts the similar trend that is observed on pure and impure $BiFeO_3$ nanocatalysts, whereby the percentage of degradation is shown to be gradually increasing at a lower dosage with a percentage of 71.43% and 69.82% for pure and impure $BiFeO_3$ nanocatalysts, respectively. The low dosage of pure $BiFeO_3$ nanocatalyst (2.5 mmol L^{-1}) is required to give optimum degradation performance up to 98% of 4-CP, whereas a higher dosage of 6.4 mmol L^{-1} of impure $BiFeO_3$ nanocatalyst is needed to achieve almost similar degradation of 4-CP (~97%). Both samples show the same trend whereby the photodegradation efficiency decreases after the optimum dosage is achieved. Previous studies have shown that this trend is caused by the high turbidity of the suspension and low light penetration [29,31].

The pure $BiFeO_3$ nanocatalyst proves to be more efficient compared to the impure $BiFeO_3$ nanocatalyst. The presence of impurities may have created the steric effect that impedes the active species from the solar-Fenton reaction. Apart from that, the efficiency of 4-CP degradation is directly affected

when ≡Fe^{2+} is affected. Hence, a higher dosage of impure $BiFeO_3$ nanocatalyst is needed to degrade the 4-CP solution.

3.2.5. Effect of the 4-CP initial concentrations on the solar-Fenton catalytic degradation of 4-CP

The effect of initial concentrations of 4-CP in the range of 50 to 300 mg L^{-1} on the solar-Fenton degradation of 4-CP is presented in Fig. 7. Both pure and impure $BiFeO_3$ nanocatalysts show similar trends whereby more than 90% degradation of 4-CP was achieved for the 4-CP concentrations of 50 to 200 mg L^{-1} after which the degradation efficiency is reduced at higher concentrations. A gradual increase in the percentage of degradation, starting from a lower concentration of 50 mg L^{-1} (89.31% and 89.70%) to a higher concentration of 200 mg L^{-1} (96.70% and 97.25%) for impure and pure $BiFeO_3$ nanocatalysts, respectively was observed. The results depicted that the pure and impure $BiFeO_3$ nanocatalysts are rather stable at higher 4-CP concentration. A sudden decrease in the percentage of degradation to ~63% is observed after the optimum concentration is achieved could be due to the insufficient H_2O_2 and ≡Fe^{2+} available to react with 4-CP molecules when the concentration was increased to more than 200 mg L^{-1}.

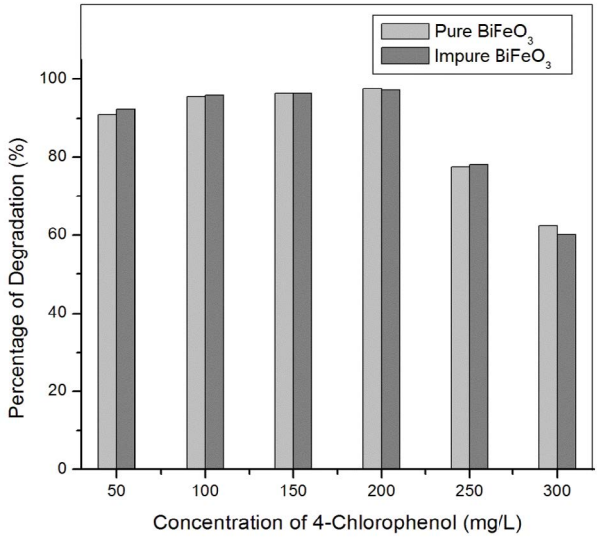

Fig. 7. Effect of initial concentration of 4-CP on solar-Fenton catalytic degradation of 4-CP. (Pure $BiFeO_3$ = 2.5 mmol L^{-1}; impure $BiFeO_3$ = 6.4 mmol L^{-1}; H_2O_2 = 0.1 mol L^{-1}; pH = 2.5; time = 180 min).

It is interesting to note, rhombohedral $BiFeO_3$ nanocatalyst exhibited 98.0% degradation efficiency of 200 mg L^{-1} 4-CP via solar-Fenton catalytic degradation within 180 min demonstrates the effectiveness of the developed photocatalyst. Compared to the relevant literature, Fenton photocatalyst, $BiFeO_3$ exhibited superior photocatalytic performance in the degradation of high concentrated 4-chlorophenol that work under direct sunlight irradiation, both in terms of the removal efficiency and the duration (Table 3). Most of the reported works for Fenton-photocatalyst, utilizing UV as a source of light. These works mostly showed the highest performance towards a low concentration of organic contaminants (≤20 ppm) with higher dosage and reaction time.

3.2.6. Kinetic study of pure and impure $BiFeO_3$ nanocatalyst on the solar-Fenton catalytic degradation of 4-CP

The photodegradation rate constant, *k*, had been assessed using the kinetic model by Langmuir-Hinshelwood. This model is a pseudo-first-kinetics model of photocatalysis and has been widely used to describe the kinetic mechanism of photocatalytic degradation of organic compounds [32]. The relationship between the rate of reaction, *r* and the concentration, *C* is expressed as follows:

$$r = -\frac{dC}{dt} = \frac{k_r K_{ad} C}{1 + K_{ad} C'} \tag{9}$$

where k_r is the intrinsic rate constant and K_{ad} is the adsorption equilibrium constant. $K_{ad}C$ is negligible when the adsorption is weak, or the adsorbate concentration is low. The adsorption kinetic equation can be simplified to the first-order model:

$$r = k_r K_{ad} C = K_{app} C \tag{10}$$

where K_{app} is the apparent adsorption constant and

$$\ln \frac{C_0}{C} = K_{app} t \tag{11}$$

Table 3
Comparison of the proposed Fenton-catalytic degradation of 4-chlorophenol with other published result

Fenton photocatalyst	Removal efficiency (%)	Light source	[4-CP] (ppm)	Catalyst dose (g L^{-1})	Reaction time (min)	References
$BiFeO_3$	98	Solar	200	0.8	180	This work
Fe_2O_3	100	UV	20	0.5	120	[34]
$FeCO_3$	100	UV	20	0.5	60	[34]
$UV/H_2O_2/Fe^{3+}$	100	UV	50	–	20	[35]
AlFePILC	100	Visible light	20	0.5	195	[36]
AlFePILC	100	UV	20	0.5	120	[36]
FeOCl/CDots	90.1	Visible light	5	1.0	180	[37]

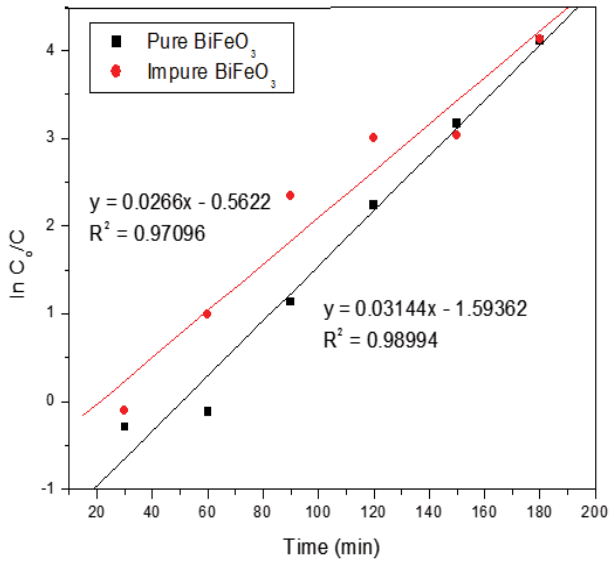

Fig. 8. Pseudo-first-order kinetic study of solar-Fenton catalytic degradation of 4-CP by (a) pure $BiFeO_3$ and (b) impure $BiFeO_3$ nanocatalyst. (Pure $BiFeO_3$ = 2.5 mmol L^{-1}; impure $BiFeO_3$ = 6.4 mmol L^{-1}; $[H_2O_2]$ = 0.1 mol L^{-1}; [4-CP] = 200 mg L^{-1}; pH = 2.5).

where C_0 is the initial 4-CP concentration and C is the concentration at time t. Thus, the values of K_{app} can be determined from the plot of $\ln C_0/C$ time against t.

The linear relationship between $\ln C_0/C$ and t for the degradation of 4-CP for pure and impure $BiFeO_3$ nanocatalysts can be observed in Fig. 8. Experimental data for both pure and impure $BiFeO_3$ nanocatalysts fit the Langmuir–Hinshelwood first-order adsorption model with a linear correlation of 0.98 and 0.957 for pure and impure $BiFeO_3$ nanocatalysts, respectively. The high correlation coefficient value (~1.0) shows a strong relationship between $\ln C_0/C$ and t. Fig. 9 shows that the degradation of 4-CP is nearly complete after 180 min for pure $BiFeO_3$ nanocatalyst, whereas the impure $BiFeO_3$ nanocatalyst requires slightly longer time, 210 min to achieve similar efficiency and the values of the rate of 4-CP degradation were 0.0314 and 0.0254 min^{-1} (Table 1) for pure $BiFeO_3$ nanocatalyst and impure $BiFeO_3$ nanocatalyst, respectively. Therefore, it is further proven that the high purity $BiFeO_3$ nanocatalyst is more effective than the impure $BiFeO_3$ nanocatalyst.

3.2.7. Regeneration of pure and impure $BiFeO_3$ nanocatalyst

Fig. 10 depicts that both pure and impure $BiFeO_3$ nanocatalyst managed to achieve up to 95% of degradation even after 5 successive cycles. The fact that the regenerated pure and impure $BiFeO_3$ nanocatalysts can be reused for subsequent degradation cycles without affecting the photocatalytic efficiency may be attributed to the easy separation of the nanocatalyst from the solution by an external magnetic field. The magnetic property of pure and impure $BiFeO_3$ nanocatalysts minimizes the loss of catalyst. 4-CP is known to be highly stable in water, thus it is desorbed from the surface of pure and impure $BiFeO_3$ nanocatalysts

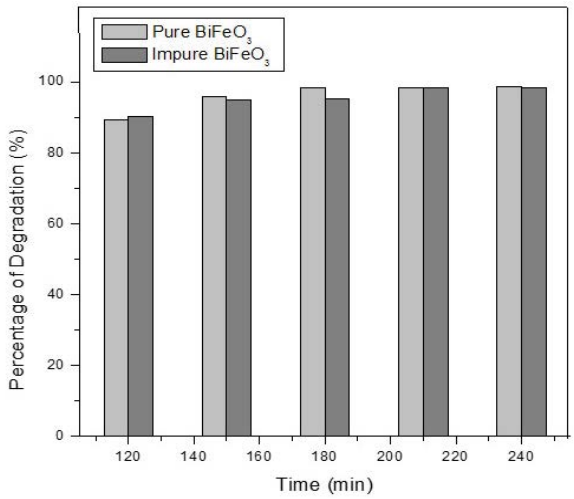

Fig. 9. Kinetic study of solar-Fenton catalytic degradation of 4-CP. (Condition: Pure $BiFeO_3$ = 2.5 mmol/L; impure $BiFeO_3$ = 6.4 mmol/L ; $[H_2O_2]$= 0.1 mol/L ; [4-CP] = 200 mg/L ; pH = 2.5).

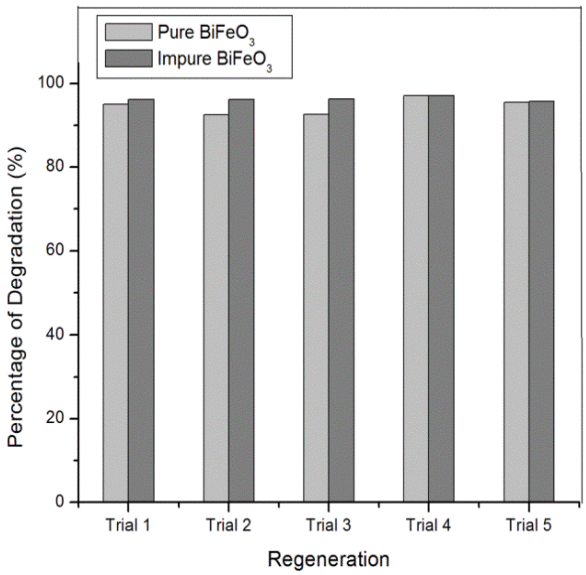

Fig. 10. Regeneration of $BiFeO_3$ nanoparticles for 5 times cycle. (Pure $BiFeO_3$ = 2.5 mmol L^{-1}; time = 180 min; impure $BiFeO_3$ = 6.4 mmol L^{-1}; time = 210 min; H_2O_2 = 0.1 mol L^{-1}; 4-CP = 200 mg L^{-1}; pH = 2.5).

simply by washing with distilled water. Therefore, this shows that both pure and impure $BiFeO_3$ nanocatalysts are highly stable, durable, and reusable.

3.3. Mineralization study

Two essential steps are involved in order to achieve complete degradation of chlorinated phenolic compounds, which are the cleavage of the aromatic ring and the removal of chlorine atom [12,33]. An adsorption–desorption equilibrium is achieved when the solution is shaken in the dark before solar irradiation, in which the solutions turn

yellowish-brown due to the formation of intermediates of chlorinated phenolic compounds. The solution then turns colorless again after 180 min, which further suggests the degradation of intermediates compounds.

Generally, the first step involved in photocatalytic degradation of 4-CP is the cleavage of the C–Cl bond that produces phenol. Then, the phenol is further attacked by •OH radicals to produce hydroquinone. However, •OH might reacts directly with 4-CP to form 4-chlorocatechol. It is worth to note that the main intermediates of 4-CP degradation are commonly known as hydroquinone and 4-chlorocatechol. As presented in Fig. 11, the UV-Vis spectrum obtained after 180 min of solar irradiation shows only a tiny peak of ~280 nm, which indicates that 4-CP is almost completely mineralized by $BiFeO_3$ nanoparticles. However, the absence of UV active intermediates did not rule out the presence of undetectable UV inactive compounds. Therefore, a further study by a more sophisticated method such as HPLC to further validate this result is essential to further verify the degree of mineralization of 4-CP by the $BiFeO_3$ nanoparticles.

4. Conclusions

In summary, the high purity of rhombohedral $BiFeO_3$ and the impure orthorhombic $Bi_2Fe_4O_9$ nanocatalyst was successfully synthesized and the performance of both catalysts was evaluated. The high purity $BiFeO_3$ nanocatalyst possesses smaller particle and crystallite size, and larger surface area compared to the impure $BiFeO_3$ nanocatalyst. The results indicated that the solar-Fenton reaction with pure $BiFeO_3$ nanocatalyst successfully removes up to ~98% of 4-CP under sunlight with the highest 4-CP concentration of 200 mg L^{-1} using 2.56 mmol L^{-1} $BiFeO_3$, 0.1 mol L^{-1} H_2O_2 at pH 2.5 within 180 min. The high purity $BiFeO_3$ nanocatalyst is more effective than the impure $BiFeO_3$ nanocatalyst due to the steric effect induced by the impurities in impure $BiFeO_3$ nanocatalyst, which requires a higher dosage of nanocatalysts and a longer reaction time. In addition to that, the nanocatalysts are reusable up to 5 consecutive cycles without a significant reduction in its degradation efficiency. In comparison with other reported work, $BiFeO_3$ promotes better degradation activity under direct sunlight irradiation towards a higher concentration of organic pollutant 4-CP. The contaminants could be removed and mineralized effectively in this system.

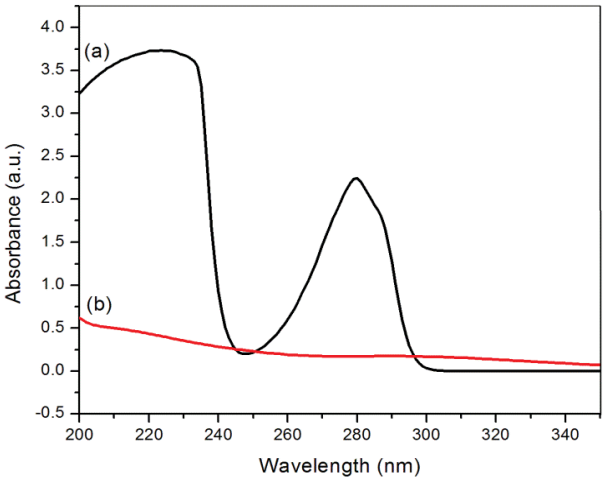

Fig. 11. UV-Vis spectra of solar-Fenton catalytic degradation of 4-CP (a) before degradation and (b) after degradation at t = 180 min using pure $BiFeO_3$ nanocatalyst.

Acknowledgment

This research was supported by the RUI grant (1001/PKIMIA/8011069) Universiti Sains Malaysia and (203.PKIMIA.6711792) by the Ministry of Higher Education Malaysia.

References

[1] A.O. Adeola, Fate and toxicity of chlorinated phenols of environmental implications: a review, Med. Anal. Chem. Int. J., 2 (2018), doi: 10.23880/macij-16000126.
[2] G.Z. Li, S.J. Park, D.-W. Kang, R. Krajmalnik-Brown, B.E. Rittmann, 2,4,5-trichlorophenol degradation using a novel TiO_2-coated biofilm carrier: roles of adsorption, photocatalysis, and biodegradation, Environ. Sci. Technol., 45 (2011) 8359–8367.
[3] A.O. Olaniran, E.O. Igbinosa, Chlorophenols and other related derivatives of environmental concern: properties, distribution and microbial degradation processes, Chemosphere, 83 (2011) 1297–1306.
[4] N. Takahashi, T. Nakai, Y. Satoh, Y. Katoh, Variation of biodegradability of nitrogenous organic compounds by ozonation, Water Res., 28 (1994) 1563–1570.
[5] A.M. Abeish, H.M. Ang, H. Znad, Solar photocatalytic degradation of chlorophenols mixture (4-CP and 2,4-DCP): mechanism and kinetic modelling, J. Environ. Sci. Health. Part A Toxic/Hazard. Subst. Environ. Eng., 50 (2015) 125–134.
[6] T.I. Poznyak, I.C. Oria, A.S. Poznyak, Ozonation and Biodegradation in Environmental Engineering: Dynamic Neural Network Approach, Elsevier, Amsterdam, The Netherlands, 2019.
[7] N.K. Temel, M. Sökmen, New catalyst systems for the degradation of chlorophenols, Desalination, 281 (2011) 209–214.
[8] R. Saravanan, F. Gracia, A. Stephen, Nanocomposites for Visible Light-induced Photocatalysis, M. Khan, D. Pradhan, Y. Sohn, Eds., Basic Principles, Mechanism, and Challenges of Photocatalysis, Springer Series on Polymer and Composite Materials, Springer, Cham, 2017, pp. 19–41.
[9] J. Schneider, M. Matsuoka, M. Takeuchi, J.L. Zhang, Y. Horiuchi, M. Anpo, D.W. Bahnemann, Understanding TiO_2 photocatalysis: mechanisms and materials, J. Am. Chem. Soc., 114 (2014) 9919–9986.
[10] S. Sakthivel, H. Kisch, Daylight photocatalysis by carbon-modified titanium dioxide, Angew. Chem. Int. Ed., 42 (2003) 4908–4911.
[11] H. Saleem, A. Habib, Study of band gap reduction of TiO_2 thin films with variation in GO contents and use of TiO_2/graphene composite in hybrid solar cell, J. Alloys Compd., 679 (2016) 177–183.
[12] Y. Mahmiani, A.M. Sevim, A. Gül, Photocatalytic degradation of 4-chlorophenol under visible light by using TiO_2 catalysts impregnated with Co(II) and Zn(II) phthalocyanine derivatives, J. Photochem. Photobiol., A, 321 (2016) 24–32.
[13] N.S. Allen, N. Mahdjoub, V. Vishnyakov, P.J. Kelly, R.J. Kriek, The effect of crystalline phase (anatase, brookite and rutile) and size on the photocatalytic activity of calcined polymorphic titanium dioxide (TiO_2), Polym. Degrad. Stab., 150 (2018) 31–36.
[14] K. Fischer, A. Gawel, D. Rosen, M. Krause, A.A. Latif, J. Griebel, A. Prager, A. Schulze, Low-temperature synthesis of anatase/rutile/brookite TiO_2 nanoparticles on a polymer membrane for photocatalysis, Catalysts, 7 (2017) 1–14, doi: 10.3390/catal7070209.

[15] A.O. Ibhadon, P. Fitzpatrick, Heterogeneous photocatalysis: recent advances and applications, Catalysts, 3 (2013) 189–218.
[16] G. Waldner, M. Pourmodjib, R. Bauer, M. Neumann-Spallart, Photoelectrocatalytic degradation of 4-chlorophenol and oxalic acid on titanium dioxide electrodes, Chemosphere, 50 (2003) 989–998.
[17] O. Avilés-García, J. Espino-Valencia, R. Romero, J.L. Rico-Cerda, R. Natividad, Oxidation of 4-chlorophenol by mesoporous titania: effect of surface morphological characteristics, Int. J. Photoenergy, 2014 (2014), https://doi.org/10.1155/2014/210751.
[18] X.Y. Li, Y. Hou, Q.D. Zhao, W. Teng, X.J. Hu, G.H. Chen, Capability of novel $ZnFe_2O_4$ nanotube arrays for visible-light induced degradation of 4-chlorophenol, Chemosphere, 82 (2011) 581–586.
[19] M.Q. Hu, Y.M. Xu, Visible light induced degradation of chlorophenols in the presence of H_2O_2 and iron substituted polyoxotungstate, Chem. Eng. J., 246 (2014) 299–305.
[20] A.B. Lavand, Y.S. Malghe, Visible light photocatalytic degradation of 4-chlorophenol using C/ZnO/CdS nanocomposite, J. Saudi Chem. Soc., 19 (2015) 471–478.
[21] K.A. Mcdonnell, N. Wadnerkar, N.J. English, M. Rahman, D. Dowling, Photo-active and optical properties of bismuth ferrite ($BiFeO_3$): an experimental and theoretical study, Chem. Phys. Lett., 572 (2013) 78–84.
[22] T. Gao, Z. Chen, Q.L. Huang, F. Niu, X.N. Huang, L.S. Qin, Y.X. Huang, A review: preparation of bismuth ferrite nanoparticles and its applications in visible-light induced photocatalyses, Rev. Adv. Mater. Sci., 40 (2015) 97–109.
[23] T. Tong, H. Zhang, J.G. Chen, D.R. Jin, J.R. Cheng, The photocatalysis of $BiFeO_3$ disks under visible light irradiation, Catal. Commun., 87 (2016) 23–26.
[24] F. Gao, X.Y. Chen, K.B. Yin, S. Dong, Z.F. Ren, F. Yuan, T. Yu, Z.G. Zou, J.-M. Liu, Visible-light photocatalytic properties of weak magnetic $BiFeO_3$ nanoparticles, Adv. Mater., 19 (2007) 2889–2892.
[25] N.A. Lomanova, V.V. Gusarov, Influence of synthesis temperature on $BiFeO_3$ nanoparticles formation, Nanosyst. Phys. Chem. Math., 4 (2013) 696–705.
[26] C. Masingboon, S. Maensiri, Synthesize, characterization and magnetic properties of nanoparticle bismuth ferrite ($BiFeO_3$) prepared by a simple sol–gel route using egg white, Ferroelectrics, 457 (2013) 89–96.
[27] M. Sivagnanavelmurugan, S. Radhakrishnan, A. Palavesam, V. Arul, G. Immanuel, Characterization of alginic acid extracted from *Sargassum wightii* and determination of its antiviral activity on shrimp *Penaeus monodon* postlarvae against white spot syndrome virus, Int. J. Curr. Res. Life Sci., 7 (2018) 1863–1872.
[28] H.A.M. Azmy, N.A. Razuki, A.W. Aziz, N.S.A. Satar, N.H.M. Kaus, Visible light photocatalytic activity of $BiFeO_3$ nanoparticles for degradation of methylene blue, J. Phys. Sci., 28 (2017) 85–103.
[29] N.A. Yusoff, L.-N. Ho, S.-A. Ong, Y.-S. Wong, W.F. Khalik, M.F. Ridzwan, Enhanced photodegradation of phenol by ZnO nanoparticles synthesized through sol–gel method, Sains Malaysiana, 46 (2017) 2507–2514.
[30] X.F. Bai, J. Wei, B. Tian, Y. Liu, T. Reiss, N. Guiblin, P. Gemeiner, B. Dkhil, I.C. Infante, Size effect on optical and photocatalytic properties in $BiFeO_3$ nanoparticles, J. Phys. Chem. C, 120 (2016) 3595–3601.
[31] M.M. Ba-Abbad, A.A.H. Kadhum, A.B. Mohamad, M.S. Takriff, K. Sopian, Photocatalytic degradation of chlorophenols under direct solar radiation in the presence of ZnO catalyst, Res. Chem. Intermed., 39 (2013) 1981–1996.
[32] N.S. Abdul Satar, R. Adnan, H.L. Lee, S.R. Hall, T. Kobayashi, M.H.M. Kassim, N.H.M. Kaus, Facile green synthesis of ytrium-doped $BiFeO_3$ with highly efficient photocatalytic degradation towards methylene blue, Ceram. Int., 45 (2019) 15964–15973.
[33] X.J. Li, J.W. Cubbage, W.S. Jenks, Photocatalytic degradation of 4-chlorophenol. 2. The 4-chlorocatechol pathway, The J. Org. Chem., 64 (1999) 8525–8536.
[34] H. Bel Hadjltaief, A. Sdiri, M.E. Gálvez, H. Zidi, P. Da Costa, M. Ben Zina, Natural hematite and siderite as heterogeneous catalysts for an effective degradation of 4-chlorophenol via photo-Fenton process, Chem. Eng., 2 (2018) 29.
[35] Y.A. Mustafa, A.H. Shihab, Removal of 4-chlorophenol from wastewater using a pilot-scale advanced oxidation process, Desal. Water Treat., 51 (2013) 6663–6675.
[36] C. Catrinescu, D. Arsene, P. Apopei, C. Teodosiu, Degradation of 4-chlorophenol from wastewater through heterogeneous Fenton and photo-Fenton process, catalyzed by Al–Fe PILC, Appl. Clay Sci., 58 (2012) 96–101.
[37] J. Zhang, G. Zhang, Q.H. Ji, H.C. Lan, J.H. Qu, H.J. Liu, Carbon nanodot-modified FeOCl for photo-assisted Fenton reaction featuring synergistic *in-situ* H_2O_2 production and activation, Appl. Catal., B, 266 (2020) 118665.

Supplementary information

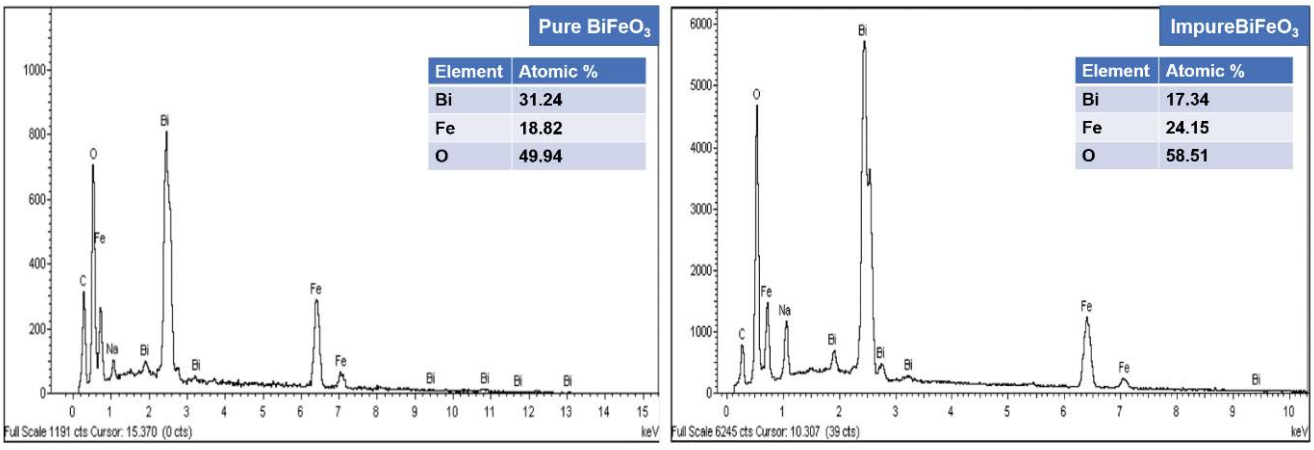

Fig. S1. Energy-dispersive X-ray analysis of pure and impure $BiFeO_3$ nanoparticles.

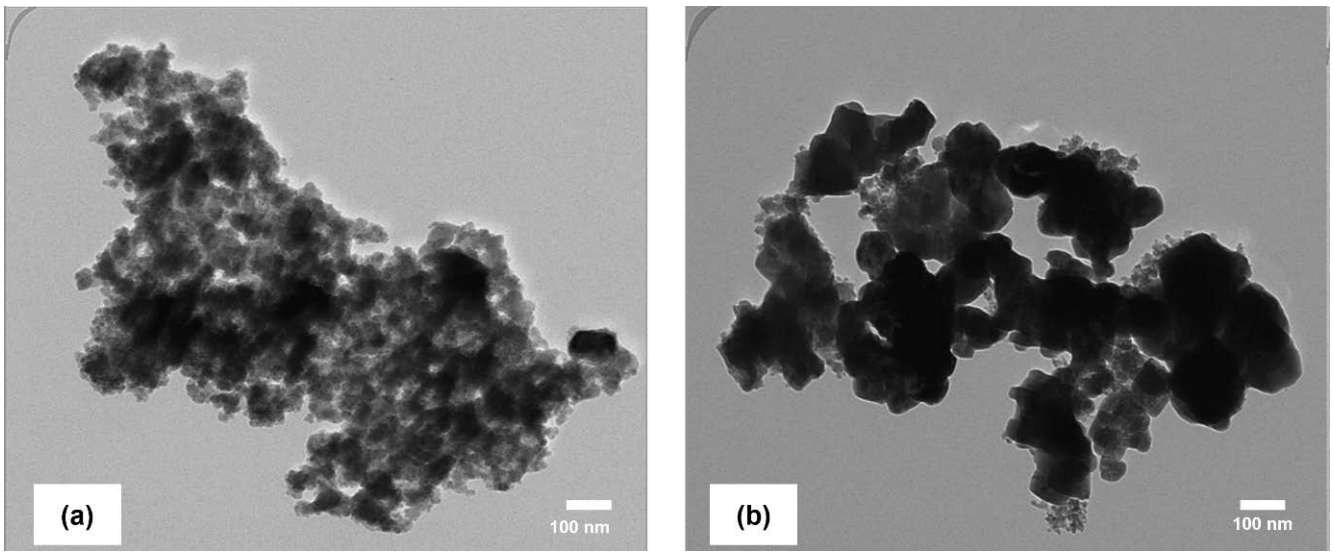

Fig. S2. Transmission electron microscopy images of (a) pure and (b) impure $BiFeO_3$ nanoparticles.